Journal of Hazardous Materials 493 (2025) 138359

Contents lists available at ScienceDirect

Journal of Hazardous Materials

journal homepage: www.elsevier.com/locate/jhazmat

The long-term *in vitro* co-exposure of polyethylene terephthalate (PET) nanoplastics and cigarette smoke condensate exacerbates the induction of carcinogenic traits

Michelle Morataya-Reyes [a], Aliro Villacorta [a,b], Javier Gutiérrez-García [a], Raquel Egea [a], Joan Martín-Pérez [a], Irene Barguilla [a], Ricard Marcos [a,*], Alba Hernández [a,*]

[a] Group of Mutagenesis, Department of Genetics and Microbiology, Faculty of Biosciences, Universitat Autònoma de Barcelona, Cerdanyola del Vallès, Barcelona, Spain
[b] Facultad de Recursos Naturales Renovables, Universidad Arturo Prat, Iquique, Chile

HIGHLIGHTS

- The coexposure effects of PET nanoplastics and tobacco condensates were evaluated.
- Long-term and human lung cells was the defined exposure scenario.
- Cancer hallmarks and transcriptomic analysys detect the induced effects.
- Co-exposure exacerbates oxidative stress, genotoxicity, and cell transformation.
- Transcriptomic analysis reveal shifts in cellular stress and key tumor-suppressor genes.

GRAPHICAL ABSTRACT

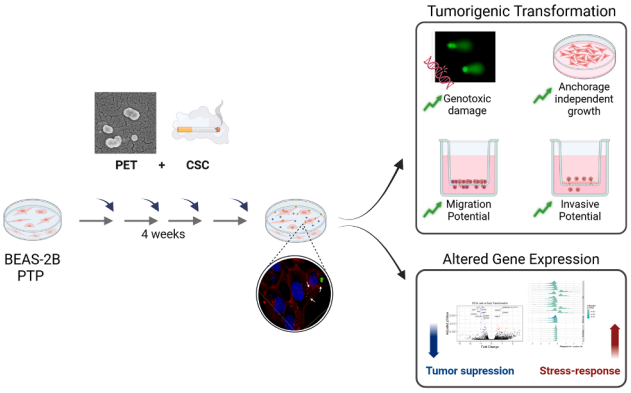

ARTICLE INFO

Keywords:
Nanoplastics
Cigarette smoke condensate
Long-term co-exposure
Beas-2B cells
Carcinogenic traits

ABSTRACT

This study examines the long-term impact of polyethylene terephthalate nanoplastics (PET-NPLs) and cigarette smoke condensate (CSC) on human lung BEAS-2B cells, focusing on key biological hallmarks of carcinogenesis. True-to-life PET-NPLs were generated from plastic water bottles and characterized to simulate environmental exposure conditions; and a comprehensive battery of assays was employed to assess genotoxicity, cellular transformation, and invasiveness. It was observed that, compared to passage control and individual exposures, co-exposure to PET-NPLs and CSC exacerbates oxidative stress, genotoxicity, and tumorigenic transformation, as evidenced by increased DNA damage, colony formation in soft agar, and enhanced cell migration and invasion. Transcriptomic analysis revealed a shift in cellular stress regulation including the upregulation of stress-response genes, including *SLC7A11, NQO1*, and *HSPA1A*, which are linked to oxidative stress adaptation and tumor survival. At the same time, key tumor-suppressor genes, such as *LOX,* and *FN1*, were significantly downregulated, promoting cellular transformation and invasiveness. These results provide compelling evidence that the

* Correspondence to: Group of Mutagenesis, Department of Genetics and Microbiology, Faculty of Biosciences, Universitat Autònoma de Barcelona, Campus of Bellaterra, Cerdanyola del Vallès, Barcelona 08193, Spain.
E-mail addresses: ricard.marcos@uab.cat (R. Marcos), alba.hernandez@uab.cat (A. Hernández).

https://doi.org/10.1016/j.jhazmat.2025.138359
Received 18 February 2025; Received in revised form 3 April 2025; Accepted 19 April 2025
Available online 21 April 2025

combination of PET-NPLs and CSC enhances carcinogenic traits through oxidative stress, genomic instability, and disruption of tumor-suppressive pathways. This study underscores the importance of evaluating the synergistic effects of combined environmental exposures and their implications for human health.

1. Introduction

The pervasive dissemination of plastics in the environment, facilitated by extensive usage and inadequate waste management practices, has emerged as a significant concern for both human health and ecosystem resilience. Particularly interesting is the environmental presence of micro- and nanoplastics (MNPLs). These environmental MNPLs result from both direct manufacturing and the fragmentation of larger plastic entities via processes such as oxidation, hydrolysis, microbial action, and mechanical abrasion [30]. Although under discussion, the present tendency is to define nanoplastics (NPLs) as those measuring 1–1000 nm, and microplastics those in the range 1–1000 mm, associating the definition to the nano/micro range of measure [24,63].

Despite the large amount of information generated during the last three years on the potential hazardous effects of MNPLs, there are four aspects requiring further research. They are i) the use of MNPLs representative (true-to-life) of those secondary MNPLs generated by plastic waste degradation. ii) To explore the effects under long-term exposure regimens, escaping from unrealistic short-time exposures. iii) To move to relevant biological endpoints such as carcinogenesis. iv) To determine the potential interactions between MNPLs and other environmental co-pollutants. Consequently, this work aims to increase our knowledge on these four topics.

Most of the information showing the harmful effects of MNPLs has been obtained using pristine commercial polystyrene MNPLs, which are far from simulating the secondary MNPLs resulting from the environmental degradation of plastic waste. Due to the difficulties of testing environmentally obtained MNPLs, the use of laboratory-made MNPLs, obtained by degrading plastic goods, is considered a good alternative [63]. Although these simulated aged MNPLs can differ from those naturally generated, they represent a step forward in closing the gap of the lack of environmental samples containing specific MNPLs. Currently, there are two main mechanisms to produce true-to-life nanoplastics, using UV-laser ablation [40] and through different mechanical fragmentation procedures, which is the most used (El [19]. By degrading polyethylene terephthalate (PET) plastic containers (including water bottles), PET-MNPLs can be obtained [27,42]; thus, this study uses true-to-life PET-NPLs obtained using such approach [64],

While acute exposure studies provide valuable insights into immediate effects, chronic exposures better capture the cumulative and potentially delayed adverse outcomes associated with NPLs exposure. This is because secondary MNPLs are present everywhere and, consequently, humans are continuously exposed to them by different routes including ingestion, inhalation, and dermal deposition. Therefore, risk assessment approaches evaluating the potential long-term effects of MNPLs exposure are urgently required [5]. Interestingly, chronic exposure studies are crucial for understanding the mechanisms underlying the development and progression of chronic diseases, including cancer. To escape using animals, an *in vitro* battery of assays covering most of the hallmarks of the carcinogenesis process has been proposed [4]. Such assays are classified as early, intermediate, or advanced biomarkers allowing the identification of the cells in the initiation, promotion, or aggressive stages of tumorigenesis. Using a pre-transformed cell model exhibiting a tumor-associated phenotype, long-term (6 months) exposures to polystyrene nanoplastics exacerbated most of the evaluated hallmarks of cancer, independently if they are associated with an early, advanced, or aggressive tumoral phenotype (Barquilla et al., 2022). It should be highlighted that the used cell model presented genetic instability, due to the presence of a mutant *Ogg1* gene. Thus, this approach permits us to identify moderated effects that could go unnoticed in the context of non-transformed cell lines or short exposure conditions, presenting a robust complementary option for assays evaluating tumorigenic potential. More recently, Domenech et al. [16] evaluated the carcinogenic potential of polyethylene terephthalate (PET-), polystyrene (PS-), and polylactic acid (PLA-) NPLs using the *in vitro* Bhas 42 cell transformation assay reporting that all three NPLs were internalized by the cells, PET- and PS-NPLs enhancing cell growth in the initiation assay. The authors also reported that PET-NPLs induced cell transformation when the promotion assay was used, indicating that PET-NPLs could act as non-genotoxic tumor promoters. These data constitute a relevant warning on the potential carcinogenic risk associated with long-term exposures to MNPLs and their potential role as co-carcinogens, when combined with tumor inducers.

Despite their small size, MNPLs exhibit complex physicochemical properties that enable them to adsorb and transport environmental pollutants, traverse biological barriers, and accumulate within living organisms [50]. Thus, the understanding of such interactions between MNPLs and environmental pollutants is of paramount relevance. Recent studies have highlighted the presence of MNPLs in urban air, with concentrations ranging from 0.3 to 1.5 particles per cubic meter, particularly in areas with high vehicular traffic and industrial activities [17]. These airborne MPLs, predominantly fibers, pose inhalation risks to urban populations. Additionally, the potential for bioaccumulation of these particles in respiratory tissues has been shown by studies reporting MPLs in lung tissue samples, with concentrations averaging 1.42 ± 1.50 particles per gram of tissue in healthy individuals [25]. When examining tumor samples, Zhao et al. [77] detected polystyrene (PS), polyethylene (PE), and polyvinyl chloride (PVC) polypropylene MPLs in 80 % of lung tumors. The presence of elevated concentrations of MNPLs in bronchoalveolar lavage fluid of smokers underscore a concerning association between smoking and microplastic inhalation [39]. Despite extensive documentation of the health hazards associated with cigarette smoking, cigarette butts persist as ubiquitous pollutants [54]. In addition to MPLs, cigarette smoke introduces complex mixtures of harmful substances, including polycyclic aromatic hydrocarbons (PAHs) and heavy metals, which can further enhance cellular uptake of microplastics and exacerbate toxic effects. The co-occurrence of MPLs and cigarette smoke in urban environments emphasizes the need to evaluate their combined health effects, as their interaction may lead to enhanced oxidative stress and genotoxicity. Thus, the simultaneous exposure to MNPLs and tobacco smoke components constitutes an expected common exposure scenario. Previous studies have shown interactions between nanoceria and cigarette smoke condensate (CSC), a known carcinogen, showing synergistic effects in different carcinogenic hallmarks in human lung epithelial cells [52], as well as inducing transforming and epigenetic cancer-like features *in vitro* [2].

Hence, the present study aims to explore the long-term carcinogenic effects of PET-NPLs in conjunction with CSC utilizing BEAS-2B cells as a model system. BEAS-2B cells, derived from human bronchial epithelium, serve as a relevant model for studying respiratory health and carcinogenesis [46]. By elucidating the interplay between PET-NPLs, CSC, and cellular responses in a long-term exposure context, this study seeks to advance our understanding of the health risks associated with NPLs pollution and allows the evaluation of PET-NPLs, previously identified as a tumor promoter agent [16], as a co-carcinogen when combined with CSC. The findings from this research may help to take regulatory decisions, risk assessment strategies, and mitigation measures aimed at reducing the adverse effects of NPLs contamination on human health and the environment.

2. Materials and methods

2.1. Particle obtention and labelling

PET-NPLs was obtained following a previously published protocol [63]. Briefly, starting from commercially available PET bottles, nanoparticles were obtained by sanding using a diamond rotary burr. The powder obtained from this process was then sieved through a 0.20 mm mesh. Four grams of the separated material were then placed on a 250 mL beaker containing a 60 ºC pre warmed trifluoroacetic acid (TFA) 90 % for 2 h or until complete dispersion on a stirring hot plate (Heidolph Instruments GmbH & Co. KG. Schwabach, Germany). The temperature was then reduced to 25 ºC, and agitation was maintained overnight. On the second day, an equal volume of TFA 20 % was carefully added to the mixture and bigger agglomerates were removed. After 24 h of stirring, the volume was transferred to glass tubes and volume was centrifuged for 1 h at 2500 rcf. Pellets were resuspended on 0.5 % sodium dodecyl sulfate (SDS) lysis buffer solution and sonicated before transferring to 250 mL graduated cylinders. The bigger fraction was allowed to settle for 1 h and the top 100 mL of each cylinder was recovered and carefully washed twice with water and pure ethanol. Clean and dry particles were then subjected to NanoGenotox protocol [43] for further biological applications.

2.2. Particle labelling

To track nanoparticles inside biological samples, PET-NPLs were labelled following our recently published protocol [62]. To proceed, a working solution of 1 mL of freshly obtained PET-NPLs at a concentration of 5 mg/mL was transferred to a glass vial containing 0.01 g of iDye Poly pink textile dye. The solution was mixed by vortexing and incubated for 2 h on a 70 ºC thermoblock. Immediately after, 9 mL of Milli-Q water were added to the solution and cleaning was carried out to eliminate the excess of dye by centrifuge using an Amicon® Ultra-15 centrifugal Ultracel®-100K filter 1 × 10 5 MWCO (Merck KGaA, Darmstadt, Germany). Shortly, 15-min centrifugations were performed at 3453 rcf, and the process was repeated a minimum of 4 times. A volume ranging from 80 to 160 µL was recovered from the V-shape well and aliquoted to volumes of 1000 µL on Milli-Q water which were maintained covered from light at 4 ºC.

2.3. PET-NPL characterization

The PET-NPLs obtained were submitted to complete analyses to confirm their physicochemical characteristics.

2.3.1. Scanning electron microscopy (SEM)

PET-NPLs were investigated by scanning electron microscopy to determine size and shape. On a sterile and clean environment, a suspension of 100 µg/mL of PET-NPLs was prepared on Milli-Q water and vigorously mixed by vortexing. A single 10 µL drop was then placed on a glass coverslip and allowed to dry overnight on a closed Petri dish. Dried particles were observed, and images were obtained on a SEM Zeiss Merlin system (Oberkochen, Germany). From the acquired images, Martin diameter was measured on 1000 random images using the ImageJ software 1.8.0_322 distribution.

2.3.2. Nanotracking analysis (NTA)

Particle size (in nm), as well as number of particles in suspension (particles per mL) were determined using a Nanosight NS300 particle analyzer from Malvern Panalytical (Cambridge, United Kingdom). Briefly, 1:50 dilutions were prepared on Milli-Q water from 100 µg/mL suspensions. The diluted suspension was mixed using a SA8 Vortex (Merck KGaA) and then 1 mL was collected on a syringe and transferred onto the Nanosight microfluidic collector on decrescent speeds from 1000 to 50 a.u. Three independent measurements were collected on a sCMOS detector using a 488 nm laser.

2.3.3. Dynamic light scattering (DLS) and zeta potential (ζ- Pot)

The particle behaviour in suspension was investigated by measuring the particle size distribution as well as the ζ- potential. Briefly, from 100 µg/mL nanoplastic suspensions the hydrodynamic behaviour or the indicative size of hard spheres that behave equivalent to the PET-NPLs suspension was evaluated by transferring 1 mL to a DTS0012 cuvette and using a dynamic light scattering (DLS) approach. The surface potential was evaluated by transferring a slightly minor volume to a DTS1070 cuvette and in both cases, measurements were carried out on a Zetasizer® Ultra red label apparatus from Malvern Panalytical (Cambridge, United Kingdom).

2.3.4. Fourier transform infrared spectroscopy (FTIR)

Functional groups from PET-NPLs were determined by FTIR. Briefly, a 20 µL drop from 1 mg/mL concentration was placed on a gold mirror and let dry for 5 days on a closed Petri dish. Sample analysis was carried out on a Hyperion 2000 micro-spectrometer (Bruker, MA, USA) using an empty gold mirror as reference. All measurements were carried out at the Molecular Spectroscopy and Optical Microscopy facility at the Institut Català de Nanociència i Nanotecnologia (ICN2). The obtained interferograms were contrasted with standard reports.

2.4. Cigarette smoke condensate (CSC) preparation

A filter pad with cigarette smoke condensate (CSC) was purchased from the University of Kentucky. CSC was prepared by the provider's 3R4F Standard Research Cigarettes on a Federal Trade Commission (FTC) smoke machine. The pad was cut into small pieces, placed in a beaker with 10 mL of DMSO (VWR, Briare, France), and mixed with a magnetic stirrer for 1 h. After removing the pieces of pad, the solution was filtered through an 11 µm-pore Whatman paper filter (GE Healthcare Life Sciences, UK) using a Bucher funnel and vacuum, and later aliquoted in cryotubes and saved at –80 ºC.

2.5. Cell culture conditions

Bronchial epithelium cells transformed with Ad12-SV40 2B (BEAS-2B), previously exposed by 30 weeks to PET-NPLs and showing cell transformation features (including increased genotoxicity, anchorage-independent growth, and deregulation of oncogenes relevant in the lung cancer context) were used as a sensitive pre-transformed cell model. These cells were generated in a study not yet published and, from now on, these cell models will be called prone-to-transformation progress (PTP) BEAS-2B cells (PTP BEAS-2B) [4]. Cells were grown in Dulbecco's modified Eagle's medium (DMEM, Life Technologies, NY, USA) supplemented with 10 % fetal bovine serum (FBS, Biowest, France), and 2.5 µg/mL of Plasmocin (InvivoGen, CA, USA). Cells were maintained in a 5 % CO_2 humidified atmosphere at 37 °C.

2.6. In vitro chronic PET-NPLs and CSC co-exposures

PTP BEAS-2B cells were exposed for 4 weeks to 100 µg/mL PET-NPLs (PTP+PET), 25 µg/mL of CSC (PTP+CSC), or the combination of both (PTP+CSC+PET), next to non-exposed passage-matched cells. A total of 1×10^5 cells were seeded in triplicate in 75 cm^2 flasks, on a total volume of 10 mL of DMEM and treated with the above indicated concentrations. Replicates of exposed cells (PTP + exposure) and non-exposed passage-matched controls (PTB) were maintained in two separate T-25 flasks and grown under the culture conditions previously described. Constant chronic exposure was ensured by replacing the cell culture medium every 3 days with a fresh medium containing the corresponding treatment.

2.7. Determination of PET-NPLs internalization in BEAS-2B cells by confocal microscopy

Confocal microscopy was used to confirm PET-NPLs internalization in PTP BEAS-2B cells using iDye staining, as recently described [62]. To proceed, after the 4 weeks of exposure 7×10^3 cells/well of each condition were seeded in an μ-Slide 8 well chambered coverslip (Ibidi GmbH, Gräfelfing, Germany), and treated with 100 μg/mL of fluorescent-labeled PET-NPLs for 48 h. After washing twice with warm culture medium, cells were observed in a Leica TCS SP5 confocal microscope. Cell nuclei were stained with Hoechst 33342 marker and cell membranes with Cellmask.

2.8. Anchorage-independent growth induction assay (Soft-agar assay)

For the evaluation of cellular transformation, the direct soft-agar assay was used to measure PTP BEAS-2B cell's ability to grow independently of anchorage. A 1:1 mix of previously liquified 1.2 % agar and DMEM 2X (DMEM, 88 mM $NaHCO_3$, 20 % FBS, 2 % non-essential amino acids, 2 % Glutamax, 2 % penicillin-streptomycin) was prepared. 1.5 mL/well of the mix was added to a 6-well plate and left to solidify overnight at 4 °C. The following day the treated cells were trypsinized and centrifuged at 1000 rpm for 8 min before discarding the supernatant and resuspending the cells in 1 mL of PBS. The cell suspension was filtered through a 40 μm mesh filter and cells were counted to determine the volume corresponding to 7.5×10^4 cells. The cells were added to 1.25 mL of DMEM, and this suspension was later mixed with 8 mL of 1:1 mix of previously liquified 1.2 % agar and DMEM 2X mix. 1.5 mL of the cell mix was added to each well with agar on the plates prepared the previous day. The cells were incubated at 37°C in a 5 % CO_2 humidified atmosphere and, after 21 d, 1 mL 1 mg/mL of 2-(4-iodophenyl)-3-(4-nitrophenyl)-5-phenyl-2H-tetrazolium (INT, Sigma-Aldrich, Germany) was added to each well and incubated for one day more. To analyze, the liquid was removed, and the plates were scanned at 1200 dpi to count the colonies per well using OpenCFU-3.9.0 software.

2.9. The comet assay

DNA damage (single strand breaks and oxidized DNA bases), resulting from exposure, was evaluated using the comet assay, with and without formamidopyrimidine DNA glycosylase (FPG) enzyme [11]. Cells were washed with PBS 1X, trypsinized, collected, and centrifuged at 300 rcf for 8 min at 4 °C. The supernatant was removed, and cells were resuspended in cold PBS at 1×10^6 cells/mL density. Cells were diluted (1:10) in 0.75 % low melting point agarose at 37 °C, and 7 μL drops of the mix were placed on Gelbond® films (GBF, Life Sciences, Vilnius, Lithuania). The films were submerged in lysis buffer (2.5 M NaCl, 0.1 M EDTA, 0.01 M Tris Base, 0.2 M NaOH, 1 % Triton X-100, 1 % N-lauroyl sarcosine, 10 % DMSO; pH 10) for 2 h at 4 °C, washed twice with enzyme buffer (0.04 m HEPES, 0.1 m KCl, 0.5 mM EDTA, 0.2 mg/mL; pH 8), and later incubated for 50 min in the same buffer. A second incubation step, with or without previously activated FPG enzyme, was done at 37 °C for 30 min. GBF were then washed with electrophoresis buffer (0.3 M NaOH, 1 mM EDTA; pH 13.4) and submerged in fresh buffer for 25 min for DNA unwinding before starting the electrophoresis (20 V, 300 mAmp, 20 min). After washing twice with cold PBS, the films were fixed in absolute ethanol and stained with 1:2500 SYBR Gold in TE buffer (10 mM Tris Base, 1 mM EDTA; pH 8). Comets were visualized using an Olympus BX50 microscope at 20 × magnification. The DNA percentage in the tail was determined with the Komet 5.5 Image analysis system (Kinetic Imaging Ltd, Liverpool, UK) as a measure of DNA damage in cells. Two samples for each triplicate of exposure treatment and control were analyzed and methyl methane sulfonate (MMS) and potassium bromate ($KBrO_3$) were used as positive controls for genotoxic and oxidative DNA damage, respectively.

2.10. Analysis of cellular senescence

Senescent cells were identified by β-galactosidase staining using the Senescence Cells Histochemical Staining Kit (Sigma-Aldrich, CS0030). Cells were seeded at 3×10^5 cells/well density in 6-well plates and stained according to the manufacturer's recommendations. The number of senescence-associated β-galactosidase-positive cells was counted using a Zeiss Axio Observer A1 microscope ($n = 6$ per treatment).

2.11. Invasion and migration induction

Invasion and migration potential were evaluated as an indirect assessment of the metastatic potential of PTP BEAS-2B after the exposure. Cells grew until the culture reached 60 % confluency before changing to serum-free DMEM for 24 h. For invasion assay, 180 μL of cold Matrigel mix (Matrigel®, 0.1 % BSA, 0.1 M NaOH) were added to each 6-well transwell insert and placed in the incubator at 37 °C and 5 % CO_2 for 1 h. Transwells were placed on a 6-well plate with 2.5 mL/well of chemoattractant medium (DMEM, 15 % FBS, 0.1 % BSA) followed by the addition of 1.5 mL of cell suspension in serum-free medium at a concentration of 2×10^5 cells/mL on top of each transwell. Cells were incubated for 48 h at 37 °C and 5 % CO_2 before fixing them with methanol and 0.2 % crystal violet. Cell invasion was evaluated by taking pictures of five different regions per transwell, using a confocal microscope Olympus FV1000, and analyzing the area covered by cells with ImageJ software 1.8.0_172. For migration assay, the same protocol was followed except for the addition of Matrigel mix to the transwells.

2.12. RNA extraction and RNA seq

After treatments, total RNA was extracted from PTP BEAS-2B cells with TRItidy G™ (AppliChem GmbH) ready-to-use solution for isolation of RNA, following the manufacturer's protocol. RNA from 2×10^6 cells was isolated and quantified for Macrogen (Korea) to perform total RNA sequencing using the Illumina NovaSeq 6000 high- throughput sequencing SBS Technology with a read length of 2×151.

2.13. Transcriptomic analysis

R version 4.3.2 was used for statistical analyses through the R Studio software [59,49]. Raw FASTQ files were quality filtered by Rfastp package [65], including sequence adapters removal, quality trimming and reads filtering below 20 bases in length. Filtered reads were mapped to the human genome GRCh38 from GENCODE and counted by Rsubread package [38,7]. Read counts from PTP cells were included in the dataset. Lowly expressed genes were filtered by the filterByExpr function and normalization between libraries was performed by calcNormFactors function, both from edgeR package [32,8]. Surrogate variants were inferred by sva package and included in the analysis [36]. Differentially expressed genes (DEGs) were obtained through limma [51] and voom [33] by contrasting the co-exposed samples (PTP+CSC+PET) and the single exposed samples. Single exposed samples included PTP and PTP + exposure samples and were combined by computing an average single-exposure value for each gene [34]. DEGs were filtered by the treat function from the limma package setting as 1.1 the minimum fold-change value to be considered meaningful.

To determine the enriched functional terms, DEGs were analyzed by STRING-db [56]. Ten predicted functional partners were added to the network. Clustering was performed by k-means clustering with 7 clusters. All genes were analyzed by gene set enrichment analysis (GSEA) performed by clusterProfiler and ReactomePA packages. Three collections were used as models: Gene Ontology (GO), MSigDB hallmark collection (h) and Reactome [14,76,71]. Parameters were left by default except for maximum gene set size on GSEA with GO which was set up to 800. Data visualization was performed by ggplot2 and ggridges packages [67,68].

2.14. Relative expression of selected DEGs using real-time RT-PCR

Following four weeks of exposure, total RNA was isolated from PTP BEAS-2B cells using TRItidy G® Reagent (Invitrogen, USA), according to the manufacturer's protocol. Residual DNA was removed with Invitrogen™ TURBO DNase™ (Thermo Fisher Scientific Baltics UAB, Lithuania), and cDNA was synthesized from 2 μg of RNA using High-Capacity RNA-to-cDNA™ Kit (Thermo Fisher Scientific Baltics UAB, Lithuania). The resulting cDNA was then analyzed by real-time PCR on a Roche LightCycler 480 to determine the relative expression levels of *SLC7A11, NQO1, HSPA11, LOX,* and *FN1*, with *β-actin* serving as the housekeeping reference. Each 20 μL reaction comprised 4 μL of cDNA (10 ng/μL), 5 μL of 2 × LightCycler 480 SYBR Green I Master (Roche, Manheim, Germany), and 0.5 μL of each primer pair at a final concentration of 500 nM. The thermal cycling conditions were 95 °C for 5 min, followed by 45 cycles of 95 °C for 10 s, 59 °C for 15 s, and 72 °C for 25 s. The primer sets were as follows: SCL7A11 f (5′- CTACTATGGTCAGAAAGCCTGT −3′) and r (5′- CAGCATAAGACAAAGCTCCAAAT −3′); NQO1 f (5′- CGGCTGGGTGTTTCAGTTTG −3′) and r (5′- GGGTGAGTTGTCAAGCCAGT −3′); HSPA11 f (5′- ATAAAAGCCCAGGGGCAAGC −3′) and r (5′- CACAGGTTCGCTCTGGGAAG −3′); LOX f (5′- AATGGAAAATCTGAAGCCCAGC −3′) and r (5′- ACCACCTTGGGCTTGATACA −3′); and FN1 f (5′- CCGCCGAATGTAGGACAAGAA −3′) and r (5′- TCCGTAGGTTGGTTCAAGCC −3′). Cycle threshold (Ct) values were generated using the LightCycler® 480 software and normalized to *β-actin* expression to obtain the fold change (2^−ΔΔCq) relative to the non-treated PTP BEAS-2B cells.

3. Results and discussion

3.1. PET-NPLs characterization

The use of representative MNPLs, that mirror environmentally ones, is a challenge when evaluating the hazards of these materials. To this date, most published studies rely on commercially available or artificially generated MNPLs, which restrict the list of materials to evaluate and may not accurately reflect the physical and chemical properties of particles found in real-life settings. The present study uses PET-NPLs derived from PET plastic water bottles and obtained through a protocol that mimics an environmental degradation process. True-to-life PET-NPLs obtained for this study are not standard materials and, for this reason, a correct characterization of its physicochemical characteristics is needed. As indicated in Fig. 1, PET-NPLs show a spherical-like shape with an average size of around 200 nm, once determined by three different methodological approaches (SEM, DLS, and NTA). Once the chemical nature was confirmed by FTITR, the ability to be properly dyed by iDye was also confirmed.

3.2. PET-NPL internalization by PTP BEAS-2B cells

The internalization of PET-NPLs particles in PTP BEAS-2B cells was visualized using confocal microscopy. As shown in Fig. 2, there were no detectable signals either in the control group (Fig. 2a) nor in the CSC-only treated group (Fig. 2b). In contrast, significant internalization was observed in the groups treated with PET-NPLs (Fig. 2c) and in the combination of CSC and PET-NPLs (Fig. 2d). This indicates that PET-NPLs can penetrate PTP BEAS-2B cells, potentially leading to intracellular accumulation and subsequent biological effects.

The ability of PET-NPLs to cross cellular membranes and accumulate intracellularly is particularly concerning given their potential to

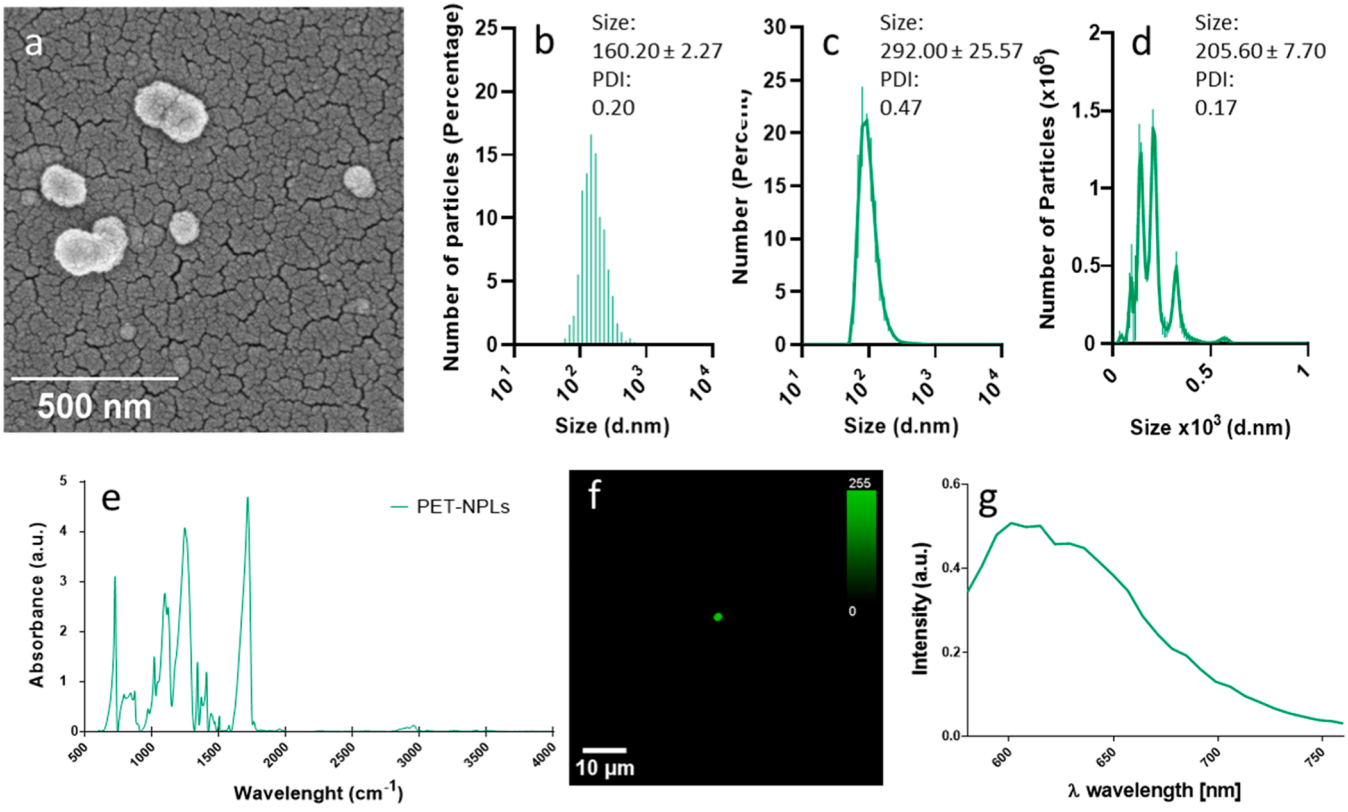

Fig. 1. SEM images of PET NPLs (a), size distribution of nanoplastic was investigated by Martin diameter measurement (b), dynamic light scattering (DLS) (c) and nanotracking analysis (NTA) (d). Chemical identity of functional groups was confirmed by Fourier transformation infrared spectroscopy (FTIR) (e). The lambda scan to detect the dying of the particles was confirmed both visually and in terms of wavelength (f and g, respectively).

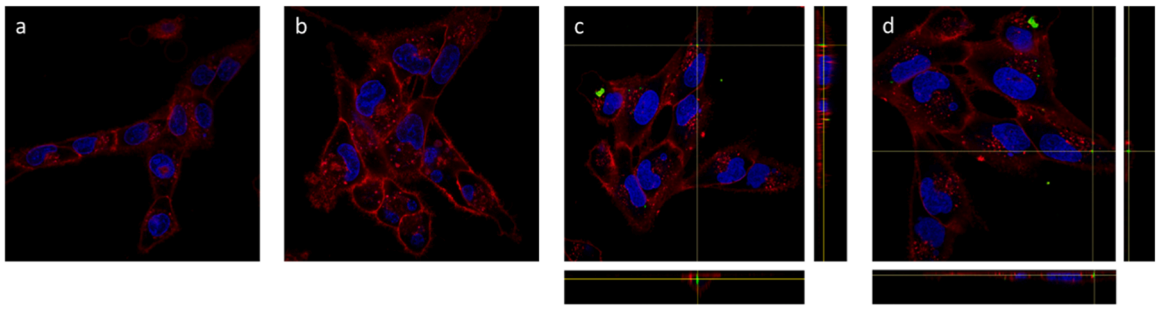

Fig. 2. Visualization of PET-NPL internalization in PTP BEAS-2B cells. a) PTP passage control. b) PTP+CSC. c) PTP+PET. d) PTP+CSC+PET. Orthogonal views of the field confirm the internalization in c) and d) after 48 h of treatment, while no PET-NPL signal is present in a) and b) conditions. Cell nuclei are shown in blue, cell membrane in red, and fluorescent-labeled LMNPET in green.

interfere with cellular processes and induce toxicological effects. Previous studies have demonstrated that the physicochemical properties of nanoplastics, such as size, shape, and surface charge, play crucial roles in their cellular uptake and bioavailability [55]. The fluorescent labeling used in this study allowed for the precise tracking of PET-NPLs particles within the cells, confirming their internalization and raising concerns about their potential to cause subcellular damage. This ability of PET-NPLs to internalize has already been demonstrated in other cell types such as primary human nasal epithelial cells [1] and human alveolar macrophages [58].

The selection of the concentrations to be used is always a conflicting issue, mainly because there is no information regarding the exposure levels of the general population. This lack of information is due to the lack of standardized protocol to quantify such levels [20]. When evaluating the obtained results, it is important to consider the difference between the treatment concentration and the effective cellular concentration. Although the used concentration (100 μg/mL) looks high, the confocal images reveal a moderated intracellular accumulation of fluorescently labeled PET-NPLs, suggesting that the particles reaching the cells are noticeably lower than the total particles treated with. This highlights a key challenge in nanoplastic exposure studies since the inconsistency between treatment and effective doses is well documented in the context of *in vitro* nanotoxicology, where factors such as particle aggregation, sedimentation, and differences in cellular uptake efficiencies influence bioavailability [12,69]. This distinction is important because it allows study bioaccumulation and long-term exposure effects in conditions where cells are not saturated with PET-NPLs, avoiding toxic effects that may accurately reflect chronic low-dose environmental exposure scenarios. By utilizing realistic, bioavailable concentrations, this study provides a relevant model for exposure to NPLs, where accumulation occurs gradually over extended periods.

3.3. Genotoxic effects of PET-NPL

Once it was determined that PET-NPLs were internalized, their potentially hazardous effects were determined. Among the biomarkers of effects genotoxicity stands out since DNA damage can severely impact cell functionality and, consequently, affect human health [6]. The comet assay was used to assess genotoxic and oxidative DNA damage in PTP BEAS-2B cells after 4 weeks of exposure to CSC, PET-NPLs, and their combination. The results, illustrated in Fig. 3, indicate that the (CSC + PET) group had significantly higher levels of DNA damage than the CSC-only and PET-only groups. These synergistic-like effects agree with previous results showing similar effects on the comet assay in co-exposures CSC + nanoceria [52]. Similarly, such co-exposure also enhanced a set of carcinogenesis biomarkers, including the overexpression of microRNAs involved in tumorigenesis [2]. These effects have been associated with the ability of CSC to induce endoplasmic reticulum stress [9]. The observed effect highlights the importance of investigating combined exposures, which may reflect more accurately real-world exposure scenarios.

Despite the effects observed when the induction of single-strand breaks was determined, no significative increases in oxidative DNA damage were found. Oxidative stress is a well-known pathway leading to genotoxicity and carcinogenesis, as it can cause mutations, lipid peroxidation, and protein oxidation [15]. The generation of reactive oxygen species (ROS) by both CSC and PET nanoplastics may lead to a compounded effect, overwhelming the cellular antioxidant defenses and resulting in significant DNA damage.

3.4. Anchorage-independent growth effects induced by PET-NPL

The cells' ability to proliferate without attachment is a key

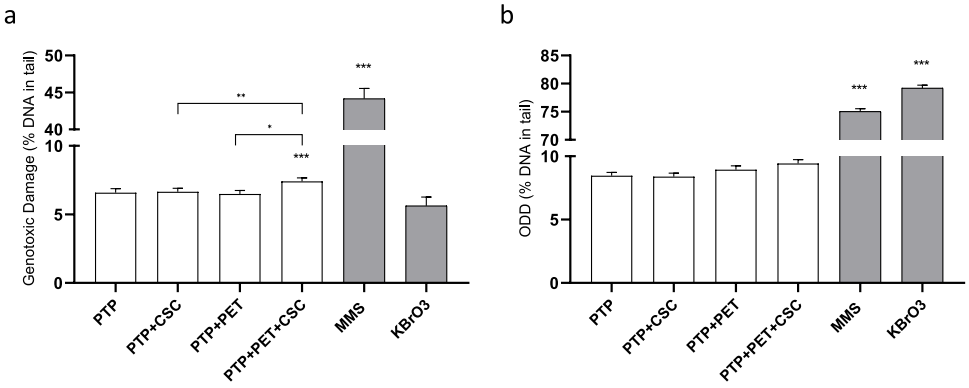

Fig. 3. (A) Genotoxic and (B) oxidative DNA damage after 4 weeks of exposure to CSC, PET, and both PET+CSC compared to PTP BEAS-2B passage control (PTP). The percentage of DNA in the tail of the comet was used to compare the conditions using one-way ANOVA analysis, with Dunnett multiple comparisons post-test and a confidence interval of 95 % (*$P \leq 0.05$; **$P \leq 0.01$, ***$P \leq 0.001$). Methyl methanesulfonate (MMS) was used as a positive control for genotoxic damage and potassium bromate ($KBrO_3$) for oxidative DNA damage.

characteristic of malignant cells, and this was assessed using the soft-agar assay [18]. Fig. 4 shows a significant increase in the total number of colonies formed in the group treated with the combination of CSC and PET-NPLs compared to the control and single treatments (Fig. 4a). The combination treatment resulted in the highest number of colonies, particularly in the smaller size range (<7 dpi), suggesting enhanced cell transformation and anchorage-independent growth (Fig. 4b).

Anchorage-independent growth is considered a hallmark of cellular transformation and is indicative of the tumorigenic potential of the tested agent [61] [4]. Our results with the soft-agar assay align with previous studies reported with silver and polystyrene nanoparticles [10, 3], and with those reporting a synergistic-like effect between CSC and nanoceria [2]. Thus, the effect observed in the co-exposure group suggests that CSC may enhance the tumorigenic properties of PET-NPLs [16] by modulating signaling pathways involved in cell adhesion and proliferation. This result also aligns with the increased genotoxic damage observed, supporting the hypothesis that chronic co-exposure to CSC and PET-NPLs accelerates the transformed phenotype in PTP BEAS-2B cells.

3.5. Migration and invasion effects induced by PET-NPL

Cell migration and invasion abilities are relevant key markers in the carcinogenic process [4]. Thus, further exploration of the potential carcinogenic phenotype using migration and invasion assays revealed significantly enhanced motility and invasive potential in PTP BEAS-2B cells exposed to PET-NPLs alone or in combination with CSC, with the highest levels observed in the co-exposure. As shown in Fig. 5a, there was a significant increase in the proportion of cells able to migrate to the basolateral side of the transwell in the groups treated with PET-NPLs and with its combination with CSC. Nevertheless, regarding the invading ability only in the co-treatments a significant effect was observed. It must be pointed out that invasion has been classified as an advanced biomarker within a battery of biomarkers measuring the progression on the transforming phenotype, while migration is classified as an intermediate biomarker [4].

Our results suggest that chronic co-exposure to CSC and PET-NPLs not only induces cellular transformation, but also enhances the invasive potential of these cells, further underscoring the carcinogenic risk posed by these combined environmental contaminants. The increased migratory and invasive capabilities observed may be attributed to several factors, including changes in the expression of matrix metalloproteinases (MMPs), alterations in the cytoskeleton, and enhanced cellular motility [10]. Thus, the combined exposure to CSC and PET-NPLs may upregulate MMP genes, particularly MMP-14, MMP-2, and MMP-9. Their respective products are key players in extracellular matrix (ECM) degradation and metastasis, facilitating cancer cell dissemination by breaking down ECM components, such as collagen and fibronectin, thereby enabling cells to breach the basement membrane and invade surrounding tissues [21] [44]. This is consistent with the enhanced invasiveness observed in the co-treatment group, where the interaction between CSC and PET-NPLs may upregulate MMP activity, thereby promoting ECM degradation and cell motility. The inflammatory tumor microenvironment induced by CSC exposure likely amplifies the pro-invasive effects of PET-NPLs. Furthermore, it has been described that the exogenously elevated levels of extracellular ATP in the ECM can increase cyclooxygenase-2 (COX-2) expression and subsequent MMP-2 activation, critical for tumor invasion [53]. Consequently, the combined exposure may enhance these pathways, further driving the invasive phenotype and aligning with previous studies showing that the combined activity of MMPs and inflammatory mediators amplifies ECM degradation and cancer cell dissemination [41].

3.6. Cellular senescence effects induced by PET-NPL

Cellular senescence, characterized by permanent cell cycle arrest and altered secretory profiles, was assessed using β-galactosidase staining. As shown in Fig. 6, β-galactosidase staining revealed a notable decrease in senescence-associated cells in the co-treatment group compared to the control and single-treatment groups. This unexpected reduction contrasts with the typical increase in senescence observed under chronic environmental stressors and warrants deeper exploration into the interplay between CSC and PET-NPLs.

The observed reduction in cellular senescence in the CSC+PET-NPLs co-exposure group aligns with emerging perspectives on the dual role of senescence in cancer [75]. While it serves as a tumor-suppressive mechanism by halting cell proliferation, it can also contribute to a pro-tumorigenic microenvironment via the senescence-associated secretory phenotype (SASP). The decreased senescence in the CSC+PET-NPLs group can indicate a suppression of SASP-driven inflammation but it could also be related to oxidative stress, altered proteostasis, or epigenetic silencing of key senescence genes [29]. This background has been observed in cases where insults converge on epigenetic regulators and in co-exposures with nanoparticles in which seemingly unrelated stressors synergize to disable signaling pathways [2,15].

Although the reduction in senescence might seem protective, it could paradoxically enhance tumorigenesis by allowing pre-malignant cells to bypass senescence and continue proliferating. The downregulation of senescence in the CSC+PET-NPLs group may reflect a shift towards other oncogenic pathways, such as those promoting cellular transformation, migration, and invasion, as evidenced by the increased anchorage-independent growth and invasive potential observed in this exposure group. This aligns with previous observations of PET-NPLs being a tumor promoter [16] and could reinforce its potential action as a co-carcinogen when in combination with established carcinogens

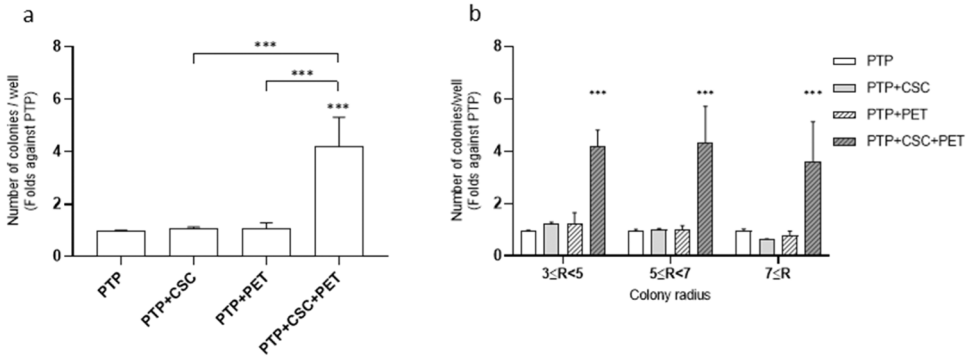

Fig. 4. Comparison of the total number of colonies formed in the anchorage-independent growth assay after treatment with CSC, PET, or the CSC + PET combination. The effects are represented as folds against non-treated PTP BEAS-2B (PTP) cells (a). The number of colonies is significantly higher in PTP BEAS-2B cells co-exposed to CSC + PET even when separating the colonies depending on size (b), represented as dpi colony radius (**$P \leq 0.001$).

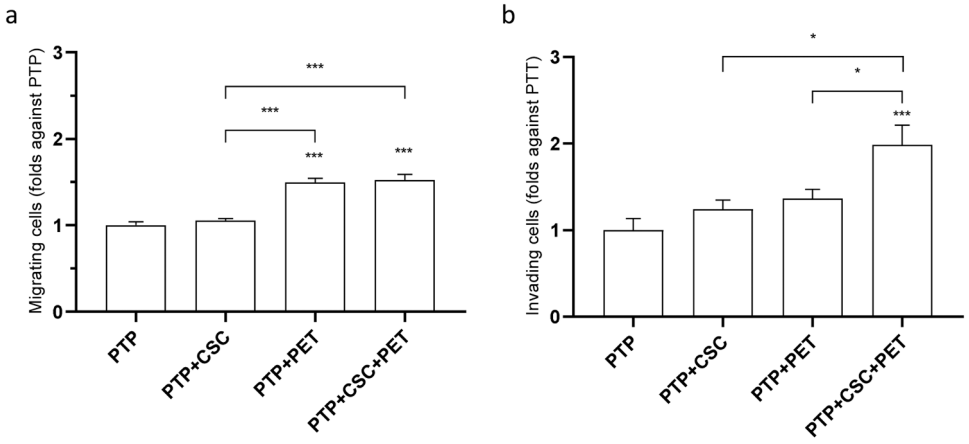

Fig. 5. The proportion of cells that can translocate to the basolateral side of the transwell in the (a) migration, and (b) invasion assays compared to PTP BEAS-2B (PTP) passage control. The folds against the PTP passage control were used to compare the effect of CSC, PET-NPLs (PET) or the combination of both in the assays using a one-way ANOVA test with Dunnett multiple comparisons post-test, having a confidence interval of 95 % (*$P \leq 0.05$; ***$P \leq 0.001$).

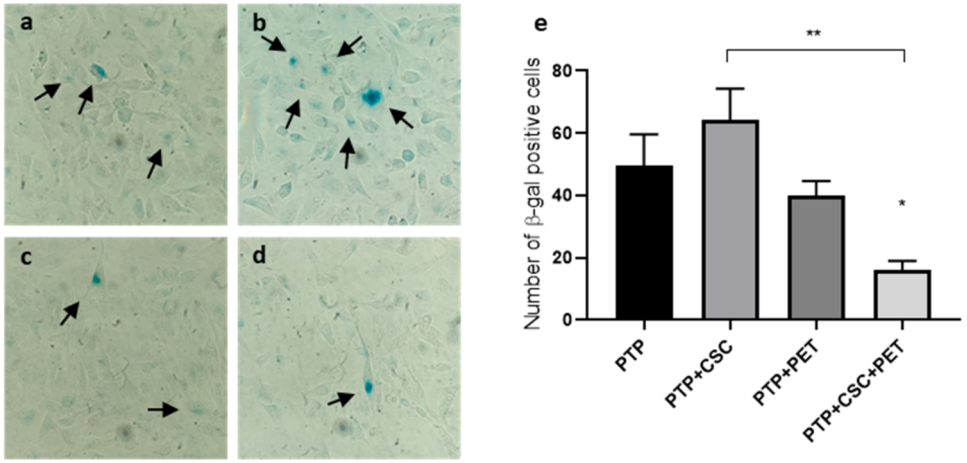

Fig. 6. Effect of CSC and PET-NPLs (PET) cotreatment in PTP BEAS-2B cells (PTP). Representative pictures of senescent cells using β-galactosidase activity in PTP control cells (a) or after 4 weeks of treatment with CSC (b), PET (c) or both CSC and PET (d). The number of β-galactosidase-positive cells (e) was significantly lower in the PTP cells co-exposed to CSC and PET when compared to the non-treated control and CSC or PET treatments alone (*$P \leq 0.05$; **$P \leq 0.01$).

such as CSC. However, further research is necessary on the mechanisms associated with the reduced senescence response examining more senescence markers and incorporating epigenetic modifications.

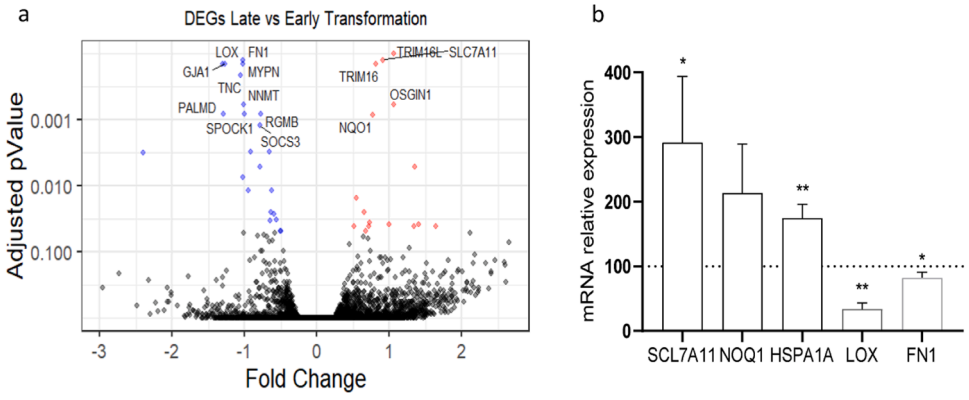

Fig. 7. (a) Volcano plot showing differentially expressed genes (DEGs) significantly up and downregulated when comparing the co-exposure treatment against the single exposure mean. Names of the most significantly expressed genes (*P* value ≤ 0.05) and those appearing in more pathways for the ORA analysis are shown. (b) Relative mRNA expression levels of *SLC7A11, NQO1, HSPA1A, LOX,* and *FN1* measured by RT-qPCR, with *β-actin* as housekeeping gene. Expression is shown as fold change ($2^{-}\Delta\Delta Cq$) relative to non-treated PTP BEAS-2B cells. Bars represent mean ± SEM of four biological replicates. $P \leq 0.05$ compared to control.

3.7. Transcriptomic analysis of the effects induced by PET-NPL and relative mRNA expression levels of DEGs

The gene expression profile of PTP BEAS-2B passage control and with treatments (alone or combined) was studied using total RNA transcriptomic analysis to determine on a broader level other effects of the exposure on PTP BEAS-2B cells. When comparing CSC + PET-NPLs co-exposed samples to single exposed samples, differentially expressed genes (DEGs) could result from differences in culture conditions and treatments. For this reason, all single-exposed samples have been combined to compute an average single-exposure value and compare it to the co-exposure value, as recommended [34].

The transcriptomic analysis revealed significant alterations in gene expression patterns in the co-exposure compared to the single-exposure group. A total of 113 DEGs were identified, with 47 upregulated and 66 downregulated genes (Fig. 7a). Notable upregulated genes include *SLC7A11, NQO1,* and *HSPA1A,* which are heavily implicated in oxidative stress management and tumor survival mechanisms.

The *SLC7A11* gene encodes a cystine-glutamate antiporter crucial for redox homeostasis, with a known role in nutrient dependency and ferroptosis regulation. Its upregulation in the co-exposure treatment presents the possibility of an adaptive response to oxidative stress promoting intracellular glutathione (GSH) synthesis, altering tumor metabolism and could contribute to therapy resistance in cancer cells [31]. This metabolic adaptation not only supports cancer cell proliferation and survival but also confers resistance to ferroptosis, a regulated form of cell death triggered by lipid peroxidation and iron accumulation [35]. Furthermore, high *SLC7A11* expression has been associated with resistance to therapies that rely on oxidative mechanisms, including radiation and certain chemotherapeutics [28]. Given its dual role in maintaining redox homeostasis and promoting therapeutic resistance, *SLC7A11* is increasingly viewed as a promising target for cancer intervention.

The *NQO1* overexpression supports detoxification and anti-oxidative stress mechanisms but also facilitates tumorigenesis in certain contexts [60]. The observed *NQO1* upregulation aligns with its role in promoting cellular proliferation and regulation of cell cycle progression at the G2/M phase related to c-Fos/CKS1 signaling [45]. Its overexpression in cancer cells has been associated with enhanced tumor cell survival under stress conditions, resistance to apoptosis, and evasion of ferroptosis, an iron-dependent form of cell death [48]. Elevated levels of *NQO1* have also been linked to increased tumorigenicity, metabolic reprogramming, and poor prognosis in various cancers, as it facilitates redox homeostasis critical for sustaining rapid cell proliferation [37]. Finally, *HSPA1A* is a member of the heat shock protein family that contributes to tumor cell survival by mitigating apoptosis and enhancing resistance to environmental stressors, was significantly upregulated [23]. Its correlation with poor prognosis in lungs, and other cancers, suggests its involvement in the enhanced malignancy observed in this study.

Conversely, key tumor-suppressor genes, such as *LOX,* and *FN1*, were downregulated in the co-exposure condition. These genes play roles in maintaining cellular adhesion and inhibiting metastatic potential, suggesting that a loss of their regulatory effects contributes to the observed aggressive phenotype. On the other hand, *LOX* and *FN1* downregulation disrupts extracellular matrix stability, favoring tumor metastasis, invasiveness, angiogenesis, and enhancing epithelial-to-mesenchymal transition [47]. As a result, the downregulation of these genes has been linked to poor clinical outcomes in various cancers [66].

To confirm these transcriptomic findings, the expression of the previously mentioned genes (*SLC711A, NQO1, HSPA1A, LOX,* and *FN1*), was validated at the mRNA level using quantitative RT-PCR. The RT-qPCR results confirmed the directionality of expression changes observed in the RNA-Seq data (Fig. 7b), providing additional robustness and biological relevance to the transcriptomic findings. This concordance strengthens the interpretation of the CSC + PET-NPLs co-exposure effects on gene expression.

Based on the identified DEGs, a STRING protein-protein interaction analysis was done with seven clusters, being "NFE2L2 regulating antioxidant/detoxification enzymes" and "Detoxification of Reactive Oxygen Species, and mRNA, protein, and metabolite induction pathway by cyclosporin A" (CsA) pathways the ones involving more DEGs (Fig. 8). It is noted that most of the proteins from the first pathway come from downregulated DEGs while the second one includes only downregulated genes. As a complementary, gene set enrichment analysis (GSEA) demonstrated significant involvement of pathways related to the detoxification of reactive oxygen species (ROS), intercellular communication, extracellular matrix (ECM) remodeling, chemoresistance and ferroptosis (Fig. 9) in CSC+PET-NPLs co-treatment. The findings shown in the ridgeplot provide insights into the complex interplay between compensatory detoxification mechanisms in the presence of combined environmental stressors. However, evaluation at a protein-level and functional assays to determine the extent of the oxidative damage are necessary to confirm its contribution to DNA damage and progression of cell transformation.

The interplay between the downregulation of Nrf2 signaling and the upregulation of CsA-associated detoxification pathways highlights a shift in cellular prioritization from prevention to damage control. While Nrf2 activation generally prevents carcinogenesis by mitigating oxidative stress and maintaining redox homeostasis, the reliance on CsA-associated pathways may reflect a state of chronic stress, wherein cells prioritize immediate survival over long-term genomic stability [13,57]. This shift has significant implications for tumorigenesis. Chronic reliance on compensatory pathways may lead to metabolic and genomic instability, creating a microenvironment conducive to malignant transformation. Furthermore, the activation of CsA-associated pathways has been linked to increased cellular motility and invasive potential, both of which are hallmarks of cancer progression [72]. The dual modulation presented by the transcriptomic analysis aligns with the enhanced cell transformation phenotype observed in the biological assays when the cells are exposed to both CSC and PET-NPLs.

Recent studies have deepened our understanding of the molecular responses of BEAS-2B cells to cigarette smoke and synthetic particles, offering relevant insights into the mechanisms potentially driving the observed phenotypes in our co-exposure model. Xu et al. [74] demonstrated that cigarette smoke extract (CSE) induces inflammation and fibrosis in BEAS-2B cells through dysregulation of the MMP-9/TIMP-1 signaling axis, which plays a critical role in extracellular matrix remodeling, while Wu et al. [70] showed that CSE exposure disrupts cell proliferation and migration via the miR-130a/Wnt1 axis. This supports our findings of deregulated transcriptomic pathways linked to cellular adhesion and communication, further emphasizing the cumulative stress induced by co-exposure. Importantly, polystyrene-based micro- and nanoparticles have also been shown to induce autophagic cell death in BEAS-2B cells [26], highlighting the cytotoxic potential of synthetic particles independently of chemical co-contaminants. Collectively, these studies contextualize our results, supporting the idea that chronic co-exposure to PET-NPLs and CSC can synergistically affect multiple cellular pathways associated with tumor initiation, tissue remodeling, and stress adaptation, reinforcing the carcinogenic potential observed in the present long-term exposure framework.

The present study provides valuable insights into the long-term co-exposure effects of PET-NPLs and cigarette smoke condensate (CSC) on PTP BEAS-2B cells, however, limitations should be acknowledged, starting from the challenge that represents the lack of standardized methods for quantifying human exposure levels to NPLs. Although several studies have detected microplastics in lung tissue and bronchoalveolar lavage fluid, no experimental data exists on the actual concentration of nanoplastics in the human respiratory system due to these analytical limitations. Additionally, while this study proves the importance of *in vitro* models as part of new approach methodologies that complement certified assays, such as the OECD's BHAS-42 assay, it is important to recognize that these models cannot replicate the full

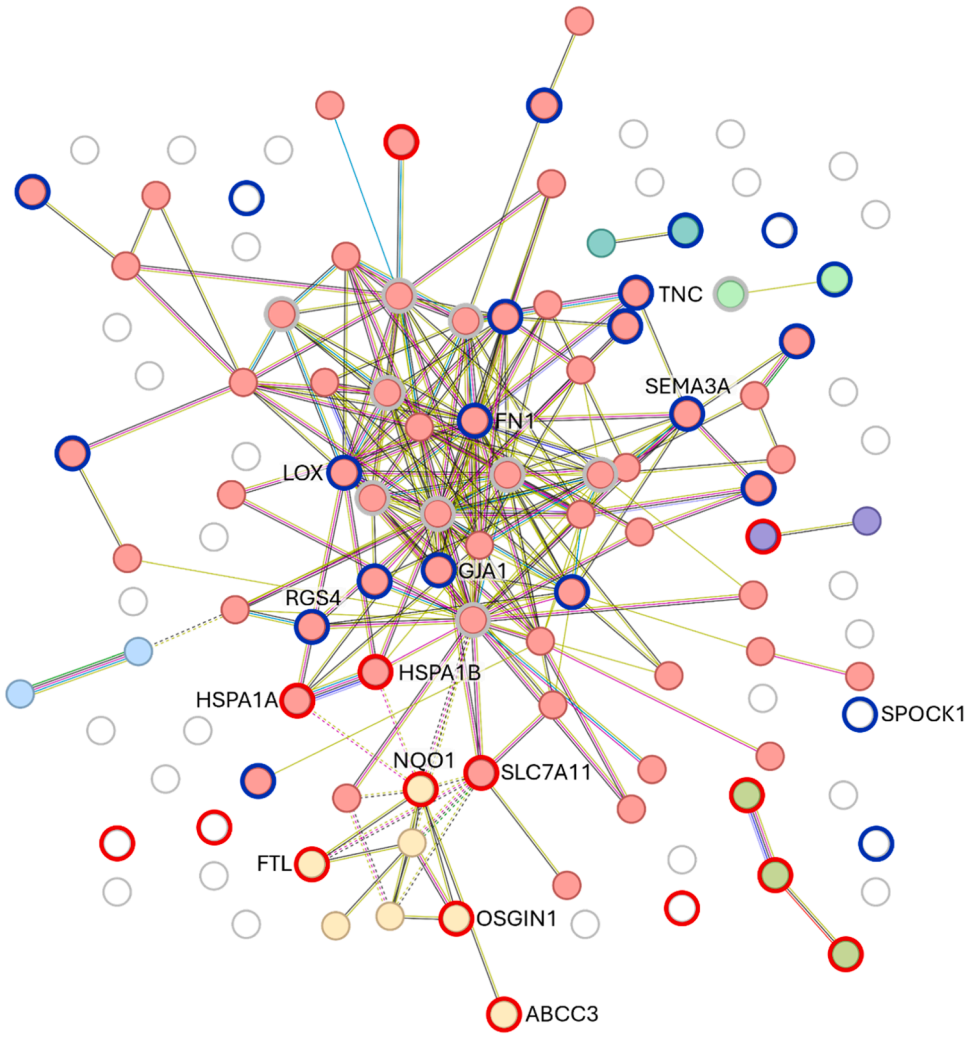

Fig. 8. String analysis of the DEGs up and downregulated in the CSC + PET co-treatment against the single exposure mean. Seven different clusters appear, including "NFE2L2 regulating antioxidant/detoxification enzymes" and "Detoxification of Reactive Oxygen Species, and mRNA, protein, and metabolite induction pathway by cyclosporin A" pathways in yellow. Upregulated and downregulated DEGs from the analysis are highlighted in red, or blue, respectively.

complexity of *in vivo* exposure scenarios, including immune system interactions and physiological clearance mechanisms.

Furthermore, the study uses only a single concentration of PET-NPLs (100 μg/mL) and CSC (25 μg/mL), selected based on prior evidence showing that these doses do not saturate the cells with nanoparticle uptake. Confocal microscopy confirmed that internalization does not occur across the total of the cell population, which supports the relevance of this dose for studying chronic bioaccumulation without inducing artificial toxicity. This scenario confirms that NPLs dosimetry remains a persistent challenge for *in vitro* studies. The effective dose reaching the cells may be significantly lower than the nominal dose due to agglomeration, sedimentation, and heterogeneous particle behavior, highlighting the need for continued efforts to improve present dosimetry models in nanotoxicology.

Another point to be highlighted in this study is the observed synergistic interaction between PET-NPLs and CSC, as indicated by the effects on different biomarkers of cell transformation and by the expression of genes involved in the tumoral response. Synergistic effects of airborne pollutants in BEAS-2B cells have been reported, as in the study of Wu et al. [73] who observed increased effects, such as intracellular ROS and inflammation, in the co-exposure of silica nanoparticles and benzo(α) pyrene after long-term (30 passages) exposure conditions. Similar effects were observed in the co-exposure of cerium NPLs and CSC, where co-exposed cells exhibit cell transforming potential, with significantly increased invasion and tumorsphere formation abilities; in addition of a high impact on a battery of miRNAs [2]. Synergistic effects have also been observed in another type of human bronchial epithelial cells (HBEC3-KT) where combined exposure to diesel exhaust particles and mineral particles induced increases in pro-inflammatory cytokines and expression of genes related to inflammation and redox responses [22]. All this emphasizes the need for further studies focusing on co-exposures to detect potential synergistic effects useful to understanding the potential health effects of such types of exposure, mainly in a long-term exposure scenario.

4. Conclusions

This study provides critical insights into the potential health risks associated with combined exposure to PET-NPLs and CSC, which are likely common in real-world scenarios. Using PTP BEAS-2B cells as a model system, it was demonstrated that long-term co-exposure exacerbates genotoxic damage, and tumorigenic traits, surpassing the effects of individual treatments. The findings are underscored by significant transcriptomic alterations, with upregulation of genes linked to management and downregulation of tumor-suppressor pathways, reflecting the complex molecular interplay induced by combined stressors.

Key results include enhanced DNA damage, anchorage-independent growth, and invasiveness, supported by disrupted antioxidant defenses

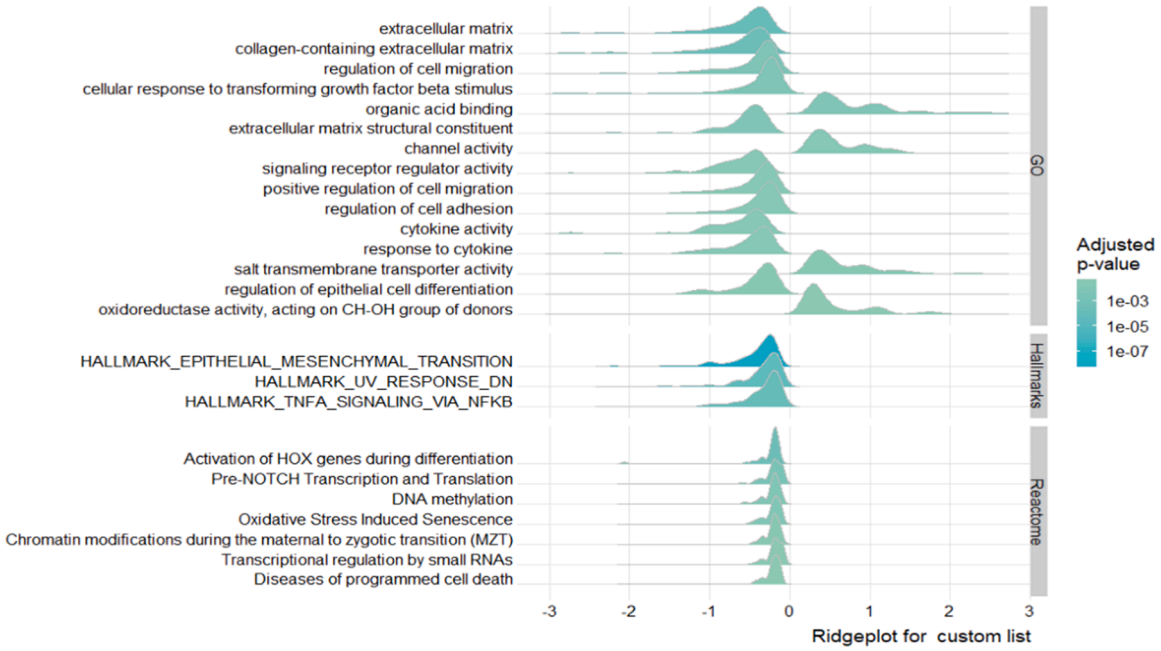

Fig. 9. Ridgeplot for list of significantly up and downregulated pathways from the GSEAs analysis of the co-treatment against the single-exposure treatments. GO, Hallmarks and Reactome databases were used and the pathways with the highest significance were included.

(e.g., *NFE2L2* downregulation) and compensatory mechanisms (e.g., cyclosporin A-mediated detoxification). These outcomes not only advance the understanding of the carcinogenic potential of nanoplastics in the presence of co-pollutants but also highlight the need for regulatory frameworks addressing such contaminants and their combined exposures. This study also becomes a step for future research to focus on elucidating molecular mechanisms further and developing targeted mitigation strategies to protect public health from the compounded effects of MNPLs and other environmental co-pollutants.

These findings underscore the value of *in vitro* long-term exposure studies and contribute to a growing body of evidence supporting the carcinogenic potential of MNPLs under realistic exposure conditions.

Environmental implication

Co-exposures is an understudied field in environmental carcinogenesis. This is especially relevant for micro/nanoplastics, as new emergent environmental contaminants, and tobacco smoke components, as a classical environmental carcinogen. In the environment, exposures last for a long time and, consequently, long-term exposure conditions need to be considered as a realistic exposure scenario. Under such conditions we have demonstrated that this co-exposure exacerbates oxidative stress, genotoxicity, and tumorigenic transformation. In addition, alter the expression of stress-response genes and key tumor-suppressor genes. Our data constitutes a relevant warning on the potential carcinogenic risk of micro/nanoplastics when co-existing with other well-known environmental toxicants.

k of micro/nanoplastics when co-exist with other well-known environmental toxicants.

CRediT authorship contribution statement

Hernández Alba: Writing – review & editing, Supervision, Funding acquisition, Conceptualization. **Marcos Ricard:** Writing – review & editing, Supervision, Conceptualization. **Villacorta Aliro:** Methodology, Investigation. **Morataya-Reyes Michelle:** Writing – original draft, Investigation, Conceptualization. **Egea Raquel:** Methodology, Investigation. **Gutiérrez-García Javier:** Investigation. **Barguilla Irene:** Methodology, Investigation. **Martín-Pérez Joan:** Methodology, Investigation.

Author statement

RM and AH planned the experiments. MMR wrote the first manuscript. MMR, AV, JGG, and JMP carried out the experimental part. MMR, RE, JGG, and IB analyzed the data, carried out the statistical analysis, and prepared tables/figures. MMR, RM, and AH wrote the final manuscript.

Declaration of Competing Interest

The authors declare that they have no known competing financial interests or personal relationships that could have appeared to influence the work reported in this paper.

Acknowledgments

MMR and JMP hold Ph.D. fellowships from the Generalitat de Catalunya. JGG holds a PIF Ph.D. fellowship from the Universitat Autònoma de Barcelona. AV was supported by a Ph.D. fellowship from the National Agency for Research and Development (ANID), CONICYT PFCHA/DOCTORADO BECAS CHILE/2020–72210237. IB (Academic record 2023-BP-00212) was granted with a Beatriu de Pinós Postdoctoral Program from the Secretariat of Universities and Research of the Department of Business and Knowledge of the Government of Catalunya. AH was granted an ICREA ACADEMIA award. This project (PlasticHeal) has received funding from the European Union's Horizon 2020 research and innovation programme under grant agreement No 965196. This work was partially supported by the Spanish Ministry of Science and Innovation [PID2020–116789, RB-C43] and the Generalitat de Catalunya (2021-SGR-00731).

Data availability

Data will be made available on request.

References

[1] Annangi, B., Villacorta, A., Vela, L., Tavakolpournegari, A., Marcos, R., Hernández, A., 2023. Effects of true-to-life PET nanoplastics using primary human nasal epithelial cells. Environ Toxicol Pharm 100, 104140. https://doi.org/10.1016/j.etap.2023.104140.

[2] Ballesteros, S., Barguilla, I., Marcos, R., Hernández, A., 2021. Nanoceria, alone or in combination with cigarette-smoke condensate, induces transforming and epigenetic cancer-like features *in vitro*. Nanomedicine 16 (4), 293–305. https://doi.org/10.2217/nnm-2020-0367.

[3] Barguilla, I., Domenech, J., Ballesteros, S., Rubio, L., Marcos, R., Hernández, A., 2022. Long-term exposure to nanoplastics alters molecular and functional traits related to the carcinogenic process. J Hazard Mater 438, 129470. https://doi.org/10.1016/j.jhazmat.2022.129470.

[4] Barguilla, I., Maguer-Satta, V., Guyot, B., Pastor, S., Marcos, R., Hernández, A., 2023. *In vitro* approaches to determine the potential carcinogenic risk of environmental pollutants. Int J Mol Sci 24 (9), 7851. https://doi.org/10.3390/ijms24097851.

[5] Brachner, A., Fragouli, D., Duarte, I.F., Farias, P.M.A., Dembski, S., Ghosh, M., Barisic, I., Zdzieblo, D., Vanoirbeek, J., Schwabl, P., Neuhaus, W., 2020. Assessment of human health risks posed by nano-and microplastics is currently not feasible. Int J Environ Res Public Health 17 (23), 8832. https://doi.org/10.3390/ijerph17238832.

[6] Carbone, M., Arron, S.T., Beutler, B., Bononi, A., Cavenee, W., Cleaver, J.E., Croce, Jr.C.M., et al., 2020. Tumour predisposition and cancer syndromes as models to study gene-environment interactions. Nat Rev Cancer 20 (9), 533–549. https://doi.org/10.1038/s41568-020-0265-y.

[7] Carlson M. *org.Hs.eg.db:* Genome wide annotation for Human (R package version 3.18.0). 2023. Retrieved from ⟨https://www.bioconductor.org/packages/org.Hs.eg.db⟩.

[8] Chen, Y., Chen, L., Lun, A., Baldoni, P., Smyth, G., 2024. edgeR 4.0: Powerful differential analysis of sequencing data with expanded functionality and improved support for small counts and larger datasets. bioRxiv. https://doi.org/10.1101/2024.01.21.576131.

[9] Chien, C.Y., Chen, Y.C., Lee, C.H., Wu, J.R., Huang, T.W., Huang, R.Y., Cheng, W. C., Hsieh, A.C., Shieh, Y.S., 2021. Dysregulation of the miR-30a/BiP axis by cigarette smoking accelerates oral cancer progression. Cancer Cell Int 21 (1), 578. https://doi.org/10.1186/s12935-021-02276-1.

[10] Choo, W.H., Park, C.H., Jung, S.E., Moon, B., Ahn, H., Ryu, J.S., Kim, K., Lee, Y.H., Yu, I.J., Oh, S.M., 2016. Long-term exposures to low doses of silver nanoparticles enhanced *in vitro* malignant cell transformation in non-tumorigenic BEAS-2B cells. Toxicol Vitr 37, 41–49. https://doi.org/10.1016/j.tiv.2016.09.003.

[11] Collins, A., et al., 2023. Measuring DNA damage with the comet assay: a compendium of protocols. Nat Protoc 18, 929–989. https://doi.org/10.1038/s41596-022-00754-y.

[12] DeLoid, G.M., Cohen, J.M., Pyrgiotakis, G., Demokritou, P., 2017. Preparation, characterization, and *in vitro* dosimetry of dispersed, engineered nanomaterials. Nat Protoc 12 (2), 355–371. https://doi.org/10.1038/nprot.2016.172.

[13] Dinkova-Kostova, A.T., Abramov, A.Y., 2015. The emerging role of Nrf2 in mitochondrial function. Free Radic Biol Med 88, 179–188. https://doi.org/10.1016/j.freeradbiomed.2015.04.036.

[14] Dolgalev, I., 2022. msigdbr: MSigDB Gene Sets Mult Org a Tidy Data Format. Retrieved from. ⟨https://CRAN.R-project.org/package=msigdbr⟩.

[15] Domenech, J., Cortés, C., Vela, L., Marcos, R., Hernández, A., 2021. Polystyrene nanoplastics as carriers of metals. interactions of polystyrene nanoparticles with silver nanoparticles and silver nitrate, and their effects on human intestinal Caco-2 cells. Biomolecules 11 (6), 859. https://doi.org/10.3390/biom11060859.

[16] Domenech, J., Villacorta, A., Ferrer, J.F., Llorens-Chiralt, R., Marcos, R., Hernández, A., Catalán, J., 2024. *In vitro* cell-transforming potential of secondary polyethylene terephthalate and polylactic acid nanoplastics. J Hazard Mater 469, 134030. https://doi.org/10.1016/j.jhazmat.2024.134030.

[17] Dris, R., Gasperi, J., Saad, M., Mirande, C., Tassin, B., 2016. Synthetic fibers in atmospheric fallout: a source of microplastics in the environment? Mar Pollut Bull 104, 290–293. https://doi.org/10.1016/j.marpolbul.2016.01.006.

[18] Du, F., Zhao, X., Fan, D., 2017. Soft agar colony formation assay as a hallmark of carcinogenesis. Bio-Protoc 7 (12), e2351. https://doi.org/10.21769/BioProtoc.2351.

[19] El Hadri, H., Gigault, J., Maxit, B., Grassl, B., Reynaud, S., 2020. Nanoplastic from mechanically degraded primary and secondary microplastics for environmental assessments. NanoImpact 17, 100206. https://doi.org/10.3390/ijerph18062997.

[20] Gigault, J., Davranche, M., 2025. Nanoplastics in focus: exploring interdisciplinary approaches and future directions. NanoImpact 37, 100544. https://doi.org/10.1016/j.impact.2025.100544.

[21] González-Ávila, G., Sommer, B., Mendoza-Posada, D., Ramos, C., Garcia-Hernandez, A., Falfán-Valencia, R., 2019. Matrix metalloproteinases participation in the metastatic process and their diagnostic and therapeutic applications in cancer. Crit Rev Oncol Hematol 137, 57–83. https://doi.org/10.1016/J.CRITREVONC.2019.02.010.

[22] Grytting, V.S., Chand, P., Låg, M., Øvrevik, J., Refsnes, M., 2022. The pro-inflammatory effects of combined exposure to diesel exhaust particles and mineral particles in human bronchial epithelial cells. Part Fibre Toxicol 19 (1), 14. https://doi.org/10.1186/s12989-022-00455-0.

[23] Guan, Y., Zhu, X., Liang, J., Wei, M., Huang, S., Pan, X., 2021. Upregulation of HSPA1A/HSPA1B/HSPA7 and downregulation of HSPA9 were related to poor survival in colon cancer. Front Oncol 11, 749673. https://doi.org/10.3389/fonc.2021.749673.

[24] Hartmann, N.B., Hüffer, T., Thompson, R.C., Hassellöv, M., Verschoor, A., Daugaard, A.E., Rist, S., Karlsson, T., Brennholt, N., Cole, M., Herrling, M.P., Hess, M.C., Ivleva, N.P., Lusher, A.L., Wagner, M., 2019. Are we speaking the same language? Recommendations for a definition and categorization framework for plastic debris. Environ Sci Technol 53 (3), 1039–1047. https://doi.org/10.1021/acs.est.8b05297.

[25] Jenner, L.C., Rotchell, J., Cowen, Benett R., Tentzeris, M., Sadofsky, V., 2022. L. Detection of microplastics in human lung tissue using μFTIR spectroscopy. Sci Total Environ 831, 154907. https://doi.org/10.1016/j.scitotenv.2022.154907.

[26] Jeon, M.S., Kim, J.W., Han, Y.B., Jeong, M.H., Kim, H.R., Sik Kim, H., Park, Y.J., Chung, K.H., 2023. Polystyrene microplastic particles induce autophagic cell death in BEAS-2B human bronchial epithelial cells. Environ Toxicol 38 (2), 359–367. https://doi.org/10.1002/tox.23705.

[27] Ji, Y., Wang, C., Wang, Y., Fu, L., Man, M., Chen, L., 2020. Realistic polyethylene terephthalate nanoplastics and the size-and surface coating-dependent toxicological impacts on zebrafish embryos. Environ Sci Nano 7 (8), 2313–2324. https://doi.org/10.1039/D0EN00464B.

[28] Jiang, Y., Sun, M., 2024. SLC7A11: the Achilles heel of tumor? Front Immunol 15, 1438807 doi: 10.3389/fimmu.2024.1438807.

[29] Jo, H., Shim, K., Jeoung, D., 2023. The potential of senescence as a target for developing anticancer therapy. Int J Mol Sci 24 (4), 3436. https://doi.org/10.3390/ijms24043436.

[30] Johannessen, C., Shetranjiwalla, S., 2021. Role of structural morphology of commodity polymers in microplastics and nanoplastics formation: fragmentation, effects and associated toxicity in the aquatic environment. Rev Environ Contam Toxicol 259, 123–169. https://doi.org/10.1007/398_2021_80.

[31] Koppula, P., Zhang, Y., Zhuang, L., Gan, B., 2018. Amino acid transporter SLC7A11/xCT at the crossroads of regulating redox homeostasis and nutrient dependency of cancer. Cancer Comm 38 (1), 1–13. https://doi.org/10.1186/s40880-018-0288-x.

[32] Law, C., Alhamdoosh, M., Su, S., Dong, X., Tian, L., Smyth, G., Ritchie, M., 2016. RNA-seq analysis is easy as 1-2-3 with limma, Glimma and edgeR. ISCB Comm J-1408 F1000Res 5. https://doi.org/10.12688/f1000research.9005.3.

[33] Law, C., Chen, Y., Shi, W., Smyth, G.K., 2014. voom: Precision weights unlock linear model analysis tools for RNA-seq read counts. Genome Biol 15, R29. https://doi.org/10.1186/gb-2014-15-2-r29.

[34] Law, C., Zeglinski, K., Dong, X., Alhamdoosh, M., Smyth, G.K., Ritchie, M.E., 2020. A guide to creating design matrices for gene expression experiments [Version 1; peer review: 2 approved]. F1000Res 9, 1444. https://doi.org/10.12688/f1000research.27893.1.

[35] Lee, J., Roh, J.-L., 2022. SLC7A11 as a gateway of metabolic perturbation and ferroptosis vulnerability in cancer. Antioxidants 11 (12), 2444. https://doi.org/10.3390/antiox11122444.

[36] Leek, J.T., Johnson, W.E., Parker, H.S., Fertig, E.J., Jaffe, A.E., Zhang, Y., Storey, J. D., Torres, L.C., 2023. sva: surrogate Variable. Anal. https://doi.org/10.18129/B9.bioc.sva. Retrieved from. ⟨https://bioconductor.org/packages/sva⟩.

[37] Li, Z., Zhang, Y., Jin, T., Men, J., Lin, Z., Qi, P., Piao, Y., Yan, G., 2015. NQO1 protein expression predicts poor prognosis of non-small cell lung cancers. BMC Cancer 15 (1), 207. https://doi.org/10.1186/s12885-015-1227-8.

[38] Liao, Y., Smyth, G.K., Shi, W., 2019. The R package Rsubread is easier, faster, cheaper and better for alignment and quantification of RNA sequencing reads. Nucleic Acids Res 47, e47. https://doi.org/10.1093/nar/gkz114.

[39] Lu, W., Li, X., Wang, S., Tu, C., Qiu, L., Zhang, H., Zhong, C., Li, S., Liu, Y., Liu, J., Zhou, Y., 2023. New evidence of microplastics in the lower respiratory tract: inhalation through smoking. Environ Sci Technol 57 (23), 8496–8505. https://doi.org/10.1021/acs.est.3c00716.

[40] Magrì, D., Sánchez-Moreno, P., Caputo, G., Gatto, F., Veronesi, M., Bardi, G., Catelani, T., Guarnieri, D., Athanassiou, A., Pompa, P.P., Fragouli, D., 2018. Laser ablation as a versatile tool to mimic polyethylene terephthalate nanoplastic pollutants: characterization and toxicology assessment. ACS Nano 12 (8), 7690–7700. https://doi.org/10.1021/acsnano.8b01331.

[41] Merchant, N., Nagaraju, G., Rajitha, B., Lammata, S., Jella, K., Buchwald, Z., Lakka, S., Ali, A., 2017. Matrix metalloproteinases: their functional role in lung cancer. Carcinogenesis 38 (8), 766–780. https://doi.org/10.1093/carcin/bgx063.

[42] Najahi, H., Alessio, N., Squillaro, T., Conti, G.O., Ferrante, M., Di Bernardo, G., Galderisi, U., Messaoudi, I., Minucci, S., Banni, M., 2022. Environmental microplastics (EMPs) exposure alter the differentiation potential of mesenchymal stromal cells. Environ Res 214 (Pt 4), 114088. https://doi.org/10.1016/j.envres.2022.114088.

[43] Nanogenotox. 2011. http://www.nanogenotox.eu/files/PDF/Deliverables/nanogenotox%20 deliverable%203_ wp4_%20dispersion%20protocol.pdf.

[44] Niland, S., Riscanevo, A., Eble, J., 2021. Matrix metalloproteinases shape the tumor microenvironment in cancer progression. Int J Mol Sci 23 (1), 146. https://doi.org/10.3390/ijms23010146.

[45] Oh, E., Kim, H., Kim, C., Lee, J., Kim, C., Lee, J., Cho, Y., Park, H., 2023. NQO1 regulates cell cycle progression at the G2/M phase. Theranostics 13, 873–895. https://doi.org/10.7150/thno.77444.

[46] Ou, W.T., Wan, Q.X., Wu, Y.B., Sun, X., Li, Y.L., Tang, D., Zhang, J., Li, S.S., Wang, N.Y., Liu, Z.L., Wu, J.J., 2024. Long noncoding RNA PSMB8-AS1 mediates the tobacco-carcinogen-induced transformation of a human bronchial epithelial cell line by regulating cell cycle. Chem Res Toxicol 37 (6), 957–967. https://doi.org/10.1021/acs.chemrestox.4c00025.

[47] Peng, D., Ungewiss, C., Tong, P., Byers, L., Wang, J., Canales, J., Villalobos, P., Uraoka, N., Mino, B., Behrens, C., Wistuba, I., Han, R., Wanna, C., Fahrenholtz, M., Grande-Allen, K., Creighton, C., Gibbons, D., 2016. ZEB1 induces LOXL2-mediated collagen stabilization and deposition in the extracellular matrix to drive lung

cancer invasion and metastasis. Oncogene 36, 1925–1938. https://doi.org/10.1038/onc.2016.358.
[48] Preethi, S., Arthiga, K., Pati, A.B., Spandana, A., Jain, V., 2022. Review on NAD(P)H dehydrogenase quinone 1 (NQO1) pathway. Mol Biol Rep 49 (9), 8907–8924. https://doi.org/10.1007/s11033-022-07369-2.
[49] R Core Team, 2023. *R: A* Language and Environment for Statistical Computing. R Foundation for Statistical Computing, Vienna, Austria. Retrieved from. ⟨https://www.R-project.org/⟩.
[50] Rafa, N., Ahmed, B., Zohora, F., Bakya, J., Ahmed, S., Ahmed, S.F., Mofijur, M., Chowdhury, A.A., Almomani, F., 2024. Microplastics as carriers of toxic pollutants: source, transport, and toxicological effects. Environ Pollut 343, 123190. https://doi.org/10.1016/j.envpol.2023.123190.
[51] Ritchie, M., Phipson, B., Wu, D., Hu, Y., Law, C., Shi, W., Smyth, G., 2015. limma powers differential expression analyses for RNA-sequencing and microarray studies. Nucleic Acids Res 43 (7), e47. https://doi.org/10.1093/nar/gkv007.
[52] Rubio, L., Bach, J., Marcos, R., Hernández, A., 2017. Synergistic role of nanoceria on the ability of tobacco smoke to induce carcinogenic hallmarks in lung epithelial cells. Nanomedicine 12 (23), 2623–2635. https://doi.org/10.2217/nnm-2017-0205.
[53] Sharma, S., Kalra, H., Akundi, R., 2021. Extracellular ATP mediates cancer cell migration and invasion through increased expression of cyclooxygenase 2. Front Pharm 11, 617211. https://doi.org/10.3389/fphar.2020.617211.
[54] Shen, M., Li, Y., Song, B., Zhou, C., Gong, J., Zeng, G., 2021. Smoked cigarette butts: Unignorable source for environmental microplastic fibers. Sci Total Environ 791, 148384. https://doi.org/10.1016/j.scitotenv.2021.148384.
[55] Stock, V., Böhmert, L., Lisicki, E., Block, R., Cara-Carmona, J., Pack, L.K., Selb, R., Lichtenstein, D., Voss, L., Henderson, C.J., Zabinsky, E., Sieg, H., Braeuning, A., Lampen, A., 2019. Uptake and effects of orally ingested polystyrene microplastic particles *in vitro* and *in vivo*. Arch Toxicol 93 (7), 1817–1833. https://doi.org/10.1007/s00204-019-02478-7.
[56] Szklarczyk, D., Kirsch, R., Koutrouli, M., Nastou, K., Mehryary, F., Hachilif, R., Gable, A., Fang, T., Doncheva, N., Pyysalo, S., Bork, P., Jensen, L., Von Mering, C., 2023. The STRING database in 2023: protein-protein association networks and functional enrichment analyses for any sequenced genome of interest. Nucleic Acids Res 51 (D1), D638–D646. https://doi.org/10.1093/nar/gkac1000.
[57] Taguchi, K., Yamamoto, M., 2020. The KEAP1–NRF2 system as a molecular target of cancer treatment. Cancers 13 (1), 46. https://doi.org/10.3390/cancers13010046.
[58] Tavakolpournegari, A., Villacorta, A., Morataya-Reyes, M., Arribas Arranz, J., Banaei, G., Pastor, S., Velázquez, A., Marcos, R., Hernández, A., Annangi, B., 2024. Harmful effects of true-to-life nanoplastics derived from PET water bottles in human alveolar macrophages. Environ Pollut 348, 123823. https://doi.org/10.1016/j.envpol.2024.123823.
[59] Team, Posit, 2023. *RStudio: Integrated Development Environment for R*. Posit Software. PBC. Retrieved from. ⟨http://www.posit.co/⟩.
[60] Tossetta, G., Fantone, S., Goteri, G., Giannubilo, S.R., Ciavattini, A., Marzioni, D., 2023. The role of NQO1 in ovarian cancer. Int J Mol Sci 24 (9), 7839. https://doi.org/10.3390/ijms24097839.
[61] Vanparys, P., Corvi, R., Aardema, M.J., Gribaldo, L., Hayashi, M., Hoffmann, S., Schechtman, L., 2012. Application of *in vitro* cell transformation assays in regulatory toxicology for pharmaceuticals, chemicals, food products and cosmetics. Mutat Res Genet Toxicol Environ Mutagen 744 (1), 111–116. https://doi.org/10.1016/j.mrgentox.2012.02.001.
[62] Villacorta, A., Cazorla-Ares, C., Fuentes-Cebrian, V., Valido, I.H., Vela, L., Carrillo-Navarrete, F., Morataya, M., Mejia-Carmona, K., Pastor, S., Velázquez, A., Arribas Arranz, J., Marcos, R., López-Mesas, M., Hernández, A., 2024. Fluorescent labeling of nanoplastics for biological applications with a focus on true-to-life MNPLs tracking. J Hazard Mater 476, 135134. https://doi.org/10.1016/j.jhazmat.2024.135134.
[63] Villacorta, A., Rubio, L., Alaraby, M., López-Mesas, M., Fuentes-Cebrian, V., Moriones, O.H., Marcos, R., Hernández, A., 2022. A new source of representative secondary PET. Nanoplastics Obtention, Charact, Hazard Eval J Hazard Mater 439, 129593 doi: 10.10.1016/j.jhazmat.2022.129593.
[64] Villacorta, A., Vela, L., Morataya-Reyes, M., Llorens-Chiralt, R., Rubio, L., Alaraby, M., Marcos, R., Hernández, A., 2023. Titanium-doped PET nanoplastics of environmental origin as a true-to-life model of nanoplastic. Sci Total Environ 880, 163151. https://doi.org/10.1016/j.scitotenv.2023.163151.
[65] Wang, W., & Carroll, T. (2024). Rfastp: An ultra-fast and all-in-one Fastq preprocessor (quality control, adapter, low quality and polyX trimming) and UMI sequence parsing (R package version 1.17.0). Bioconductor. ⟨https://bioconductor.org/packages/Rfastp⟩.
[66] Wang, T.-H., Hsia, S.-M., Shieh, T.-M., 2016. Lysyl oxidase and the tumor microenvironment. Int J Mol Sci 18 (1), 62. Doi: 10.3390/ijms18010062.
[67] Wickham, H., 2016. ggplot2: Elegant Graphics for Data Analysis. Springer-Verlag New York.
[68] Wilke C. ggridges: Ridgeline Plots in 'ggplot2' (R package version 0.5.6). 2024. Retrieved from ⟨https://CRAN.R-project.org/package=ggridges⟩.
[69] Wright, S., Cassee, F.R., Erdely, A., Campen, M.J., 2024. Micro- and nanoplastics concepts for particle and fibre toxicologists. Part Fibre Toxicol 21, 18. https://doi.org/10.1186/s12989-024-00581-x.
[70] Wu, Y., Guan, S., Ge, Y., Yang, Y., Cao, Y., Zhou, J., 2020. Cigarette smoke promotes chronic obstructive pulmonary disease (COPD) through the miR-130a/Wnt1 axis. Toxicol Vitr 65, 104770. https://doi.org/10.1016/j.tiv.2020.104770.
[71] Wu, T., Hu, E., Xu, S., Chen, M., Guo, P., Dai, Z., Feng, T., Zhou, L., Tang, W., Zhan, L., Fu, X., Liu, S., Bo, X., Yu, G., 2021. clusterProfiler 4.0: a universal enrichment tool for interpreting omics data. Innovation 2 (3), 100141.
[72] Wu, Q., Wang, X., Nepovimova, E., Wang, Y., Yang, H., Kuca, K., 2018. Mechanism of cyclosporine A nephrotoxicity: oxidative stress, autophagy, and signalings. Food Chem Toxicol 118, 889–907. https://doi.org/10.1016/j.fct.2018.06.054.
[73] Wu, J., Zhang, J., Nie, J., Duan, J., Shi, Y., Feng, L., Yang, X., An, Y., Sun, Z., 2019. The chronic effect of amorphous silica nanoparticles and benzo[a]pyrene co-exposure at low dose in human bronchial epithelial BEAS-2B cells. Toxicol Res (Camb) 8 (5), 731–740. https://doi.org/10.1039/c9tx00112c.
[74] Xu, W., Li, F., Zhu, L., Cheng, M., Cheng, Y., 2023. Pacenta polypeptide injection alleviates the fibrosis and inflammation in cigarette smoke extracts-induced BEAS-2B cells by modulating MMP-9/TIMP-1 signaling. J Biochem Mol Toxicol 37 (11), e23453. https://doi.org/10.1002/jbt.23453.
[75] Yang, J., Liu, M., Hong, D., Zeng, M., Zhang, X., 2021. The paradoxical role of cellular senescence in cancer. Front Cell Dev Biol 9, 722205. https://doi.org/10.3389/fcell.2021.722205.
[76] Yu, G., He, Q., 2016. ReactomePA: An R/Bioconductor package for reactome pathway analysis and visualization. Mol Biosyst 12 (2), 477–479. https://doi.org/10.1039/c5mb00663e.
[77] Zhao, J., Zhang, H., Shi, L., Jia, Y., Sheng, H., 2024. Detection and quantification of microplastics in various types of human tumor tissues. Ecotoxicol Environ Saf 283, 116818. https://doi.org/10.1016/j.ecoenv.2024.116818.